Journal of Materials Science & Technology 35 (2019) 2494–2502

Contents lists available at ScienceDirect

Journal of Materials Science & Technology

journal homepage: www.jmst.org

Research Article

Biofilm inhibition and corrosion resistance of 2205-Cu duplex stainless steel against acid producing bacterium *Acetobacter aceti*

Dan Liu[a,1], Ru Jia[b,1], Dake Xu[c,*], Hongying Yang[a,*], Ying Zhao[d], M. saleem Khan[e], Songtao Huang[f], Jiankang Wen[f], Ke Yang[e], Tingyue Gu[g]

[a] School of Metallurgy, Northeastern University, Shenyang, 110819, China
[b] Mary Kay O'Connor Process Safety Center, Artie McFerrin Department of Chemical Engineering, Texas A&M University, College Station, TX 77843, USA
[c] Shenyang National Laboratory for Materials Science, Northeastern University, Shenyang, 110819, China
[d] Shenzhen Institutes of Advanced Technology, Chinese Academy of Sciences, Shenzhen, 518055, China
[e] Institute of Metal Research, Chinese Academy of Sciences, Shenyang, 110016, China
[f] General Research Institute for Nonferrous Metals, Beijing, 100088, China
[g] Department of Chemical and Biomolecular Engineering, Institute for Corrosion and Multiphase Technology, Ohio University, Athens, OH 45701, USA

ARTICLE INFO

Article history:
Received 19 March 2019
Received in revised form 12 April 2019
Accepted 13 May 2019
Available online 21 June 2019

Keywords:
Duplex stainless steel
Acid producing bacteria
Microbiologically influenced corrosion
Pitting corrosion

ABSTRACT

Acid producing bacterium *Acetobacter aceti* causes pitting corrosion of stainless steel (SS). This work investigated the enhanced resistance of 2205-Cu duplex stainless steel (DSS) against biocorrosion by *A. aceti* in comparison with 2205 DSS using electrochemical and surface analysis techniques. With the addition of Cu to 2205 DSS, biofilms on the 2205-Cu DSS surface were inhibited effectively. The largest pit depth on 2205-Cu DSS surface in the presence of *A. aceti* was 2.6 μm, smaller than 5.5 μm for 2205 DSS surface. The i_{corr} was 0.42 ± 0.03 μA cm^{-2} for 2205-Cu DSS in the biotic medium, which was much lower than that for 2205 DSS (3.69 ± 0.65 μA cm^{-2}). All the results indicated that the *A. aceti* biofilm was considerably inhibited by the release of Cu^{2+} ions from the 2205-Cu DSS matrix, resulting in the mitigation of biocorrosion by *A. aceti*.

© 2019 Published by Elsevier Ltd on behalf of The editorial office of Journal of Materials Science & Technology.

1. Introduction

Duplex stainless steel (DSS) consists of ferrite phase (α) and austenite phase (γ), combining excellent corrosion resistance with high strength and good machinability [1–3]. 2205 DSS is widely used in some harsh settings such as marine applications and nuclear industry applications due to its excellent corrosion resistance [4,5]. For instance, 2205 DSS has been used for nuclear waste containers in UK [6]. However, it was reported that 2205 DSS can be corroded by microorganisms [7–10]. Corrosion is a naturally occurring phenomenon, causing great economic losses and safety issues. The global losses caused by corrosion are approximately 4 trillion dollars per year. Microbiologically influenced corrosion (MIC) contributes 20% of the total corrosion damages [11,12]. It is believed that biofilms are responsible for MIC [13–17]. Biofilm attachment can adversely affect the electrochemical conditions of the material interfaces, thus accelerating the corrosion of metals [18]. In extracellular electron transfer-MIC (EET-MIC), sessile cells in biofilms use electrons from extracellular metal oxidation for the reduction of a terminal electron acceptor (e.g., sulfate and nitrate) intracellularly under biocatalysis [13,19,20]. Microbes such as acid producing bacteria (APB) secrete corrosive metabolites (organic acids) that produce an acidic environment underneath the APB biofilm causing metal corrosion. The corrosion is caused by extracellular oxidation of the metal by the secreted corrosive acids. This is known as metabolite-MIC (M-MIC) [21,22]. Dong et al. found that aggressive acidic environment was produced by *Acidithiobacillus caldus* SM-1 used in bioleaching, thus causing severe pitting corrosion against S32654 super austenitic stainless steel [23]. Apart from the two types of MIC that are caused by microbes, microbes can also accelerate corrosion by a pre-existing corrosive agent such as CO_2 because biofilms can damage passivation films on a metal surface.

It was reported that acetic acid-producing bacteria contributed to the acceleration of corrosion of underground storage tank (UST) [24–26]. Moreover, the pitting corrosion of steel alloys and copper of UST in the presence of *Acetobacter aceti* was reported [27].

* Corresponding authors.
E-mail addresses: xudake@mail.neu.edu.cn (D. Xu), yanghy@smm.neu.edu.cn (H. Yang).
[1] The authors equally contributed to this work.

https://doi.org/10.1016/j.jmst.2019.05.048
1005-0302/© 2019 Published by Elsevier Ltd on behalf of The editorial office of Journal of Materials Science & Technology.

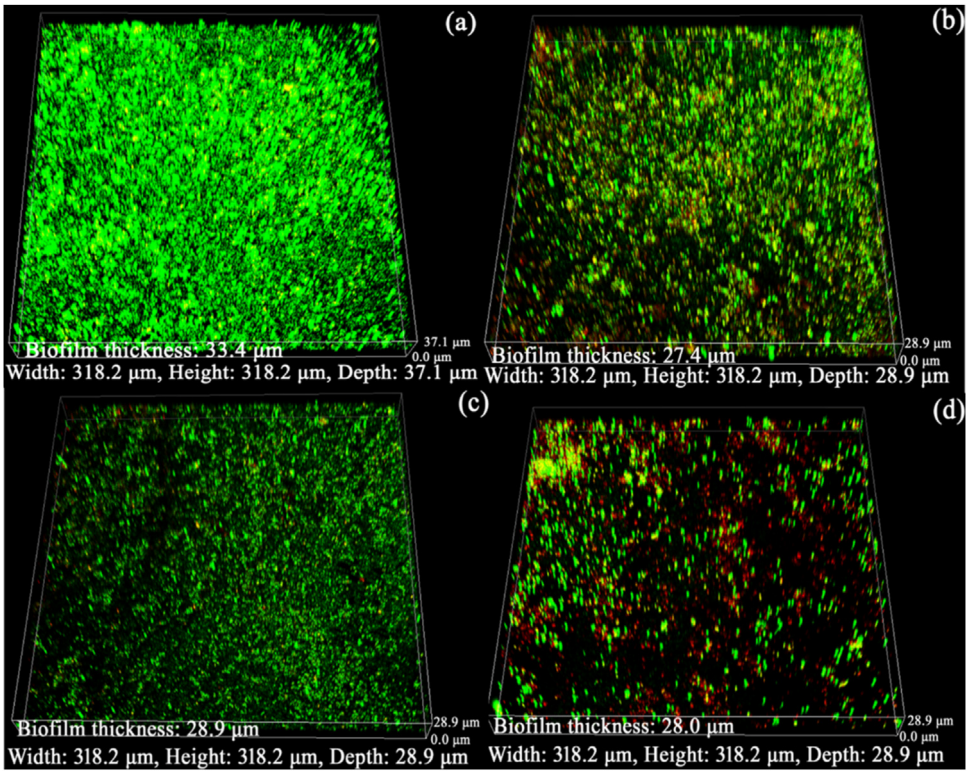

Fig. 1. CLSM images of *A. aceti* biofilm on the surface of (a) 2205 DSS after 7 days, (b) 2205-Cu DSS after 7 days, (c) 2205 DSS after 14 days, and (d) 2205-Cu DSS after 14 days.

A. aceti is a strictly aerobic, rod shaped Gram-negative bacterium [28]. It possesses the ability to produce weak organic acids by oxidizing multifarious alcohols and sugars [29,30]. Compared with strong acids, organic acids such as acetic acid are far more corrosive at the same pH [31]. Because organic acids have a buffering power to supply additional protons, which can attack metal and occur extracellularly on a metal surface [32].

It is known that copper offers excellent antibacterial properties against various microorganisms [26,28,33]. Based on this, the 2205-Cu DSS has been developed by adding Cu to 2205 DSS [9]. It has been demonstrated that the released copper ion (Cu^{2+}) from 2205-Cu DSS inhibited the biofilm formation on the metal surface, thus leading to effective mitigation of EET-MIC caused by nitrate-reducing *Pseudomonas aeruginosa* [14,34,35]. However, 2205-Cu DSS has not been reported for the mitigation of M-MIC by APB.

This work investigated the corrosion resistance of 2205-Cu DSS against acid producing bacterium *A. aceti*. Electrochemical and surface analysis methods were used to evaluate the anticorrosion behavior and antibacterial performance of 2205-Cu DSS using 2205 DSS as control.

2. Experimental

2.1. Materials and methods

Commercial 2205 DSS was purchased from Taiyuan Iron & Steel Co., Ltd., Shanxi Province, China. 2205-Cu DSS was produced by Institute of Metal Research (IMR), Chinese Academy of Sciences, Shenyang, China [35]. Table 1 lists its elemental composition (wt%) analyzed by the Department of Materials Analysis and Testing at IMR. 2205-Cu DSS coupons were annealed at 1050 °C for 1 h, then aged at 540 °C for 4 h to guarantee copper precipitation in the 2205-Cu DSS matrix. The coupons were rinsed with distilled water and dried after being abraded using silicon carbide papers sequentially from 150 to 1000 grit.

A. aceti (CGMCC 1.1809) was obtained from the China General Microbiological Culture Collection Center (CGMCC), Beijing, China. The medium used for the bacterial cultivation was composed of 100 g/L glucose, 10.0 g/L yeast extract, 20.0 g/L $CaCO_3$ and 15.0 g/L agar. All the chemicals used in the culture medium were purchased from Oxoid (Basingstoke, Hants, UK). The medium was sterilized by autoclaving for 30 min at 115 °C. The initial concentration of *A. aceti* immediately after inoculation was 10^7 cells/mL.

2.2. Electrochemical tests

Electrochemical measurements were performed in 500 mL electrochemical glass cell filled with 200 mL culture medium to submerge the electrodes. Each working electrode was soldered with copper wire and then mounted in epoxy resin with a 1 cm^2 exposed area. The counter electrode was a platinum plate (10 mm × 10 mm × 0.1 mm), and the reference electrode was a saturated calomel electrode (SCE). All the electrochemical tests, including open circuit potential (OCP), linear polarization resistance (LPR), electrochemical impedance spectroscopy (EIS) and potentiodynamic polarization were conducted using a Reference 600™ potentiostat (Gamry Instruments, Inc., PA, USA). The LPR measurements were conducted with a scan rate of 0.125 mV/s in the range from −5 mV to 5 mV vs. OCP. EIS was scanned under stable OCP with a 5 mV AC voltage amplitude in the frequency range from 10^5 Hz to 10^{-2} Hz. The data from EIS were analyzed using ZSimDemo software (EChem Software, MI, USA). The potentiodynamic polarization curves were obtained only once for each working electrode at a scan rate of 0.5 mV/s in the potential range from −500 mV to 1500 mV after the 14-day incubation period. All the experiments were repeated at least thrice to confirm the data reproducibility.

Table 1
Elemental compositions of 2205 DSS and 2205-Cu DSS (wt%).

Sample	Si	Mn	P	S	Ni	Cr	Mo	Cu	N	Fe
2205-Cu DSS	0.04	0.01	0.006	0.0034	6.03	23.63	2.90	3.02	0.23	Bal.
2205 DSS	0.51	1.14	0.03	<0.001	5.89	23.22	3.10	–	0.17	Bal.

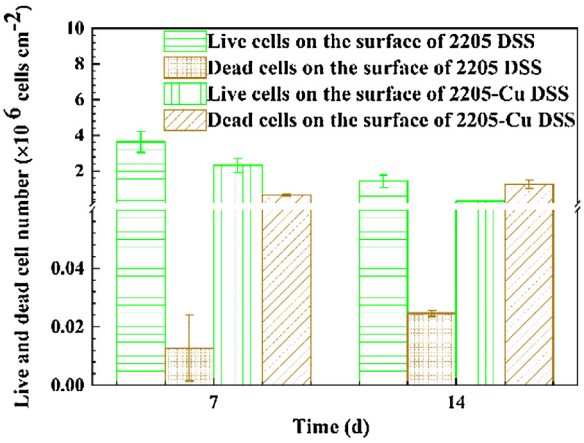

Fig. 2. Live and dead sessile cell counts on the surface of 2205 DSS and 2205-Cu DSS after 7 and 14 days.

2.3. Surface analysis

To observe *A. aceti* biofilm morphologies on coupon surfaces, field emission scanning electron microscopy (FESEM) (Ultra-Plus, Zeiss, Jena, Germany) was used. In order to analyze corrosion products on coupons, X-ray photoelectron spectroscopy (XPS, ESCALAB250, Thermo VG, MA, USA) was performed employing a monochromatic X-ray source (Al $K\alpha$ line of 15 kV and 150 W) with a pass energy of 50 eV and a step size of 0.1 eV. The wide binding energy was in the range from 0 to 1350 eV.

To investigate the antibacterial effect of 2205-Cu DSS against the *A. aceti* biofilm, live/dead staining of sessile cells were performed by following the procedure previously described by Lou et al. [36]. Biofilm images were taken with the use of a confocal laser scanning microscope (CLSM) (C2 Plus, Nikon, Tokyo, Japan). A different CLSM (LSM 710, Zeiss, Jena, Germany) was used for measuring the pit depth on the coupon surface.

2.4. Copper ion release test

The coupons with dimensions of 10 mm × 10 mm × 5 mm were used for the test. All the surfaces were covered with Teflon except a top 10 mm × 10 mm exposed surface. Three 2205-Cu DSS coupons were immersed in 100 mL medium, and the bulk solution was used to examine the copper ion released from the coupons using atomic absorption spectroscopy (AAS, Z-2000, Hitachi, Tokyo, Japan).

3. Results

3.1. Characterization of biofilm and pit depth examination

Fig. 1 shows the sessile cell densities visually by CLSM observation. After 7 days of incubation, the 2205 DSS surface had a larger maximum biofilm thickness and average biofilm thickness (33.4 μm, 29.8 ± 4.1 μm) than that on 2205-Cu DSS (27.4 μm, 26.2 ± 0.5 μm). Furthermore, some dead cells (red dots) can be seen on 2205-Cu DSS in Fig. 1(b). After 14 days of immersion, the maximum biofilm thickness was similar on both surfaces, and much more dead cells are seen on 2205-Cu DSS in Fig. 1(d). In comparison, dead cells are hard to see on 2205 DSS in Fig. 1(a, c). Fig. 2 shows the numbers of live cells and dead cells quantified using the ImageJ software (National Institutes of Health, Bethesda, MD, USA) [36]. The data in Fig. 2 confirm the antimicrobial effect of the 2205-Cu DSS.

Fig. 3 shows *A. aceti* biofilms on the surfaces of 2205 DSS and 2205-Cu DSS after 7 and 14 days. In all cases, sessile cells are seen on the metal surface with very little observable EPS (exopolymeric substances). After 7 days of immersion, there were much more sessile cells on 2205 DSS than on 2205-Cu DSS. After 14 days

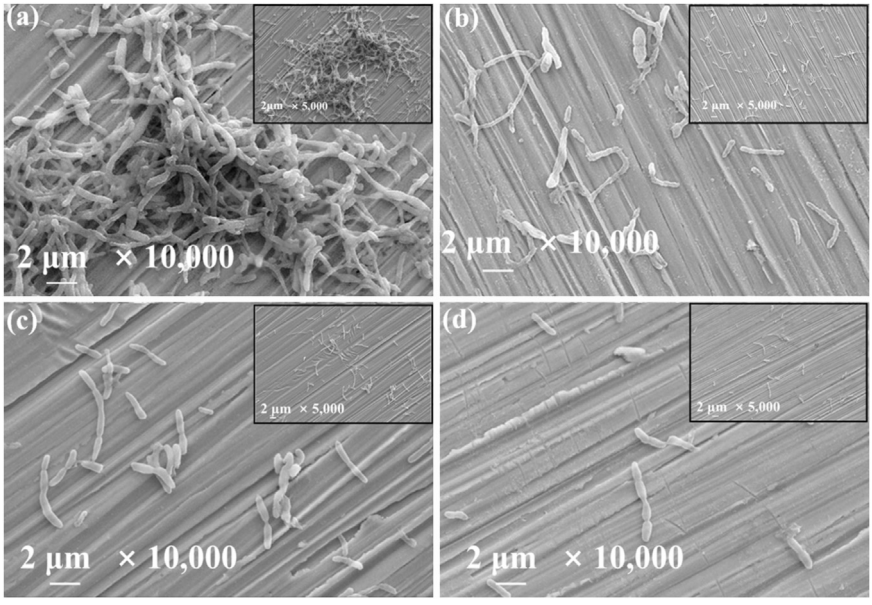

Fig. 3. SEM images of *A. aceti* biofilms on the surfaces of (a) 2205 DSS after 7 days, (b) 2205-Cu DSS after 7 days, (c) 2205 DSS after 14 days, and (d) 2205-Cu DSS after 14 days.

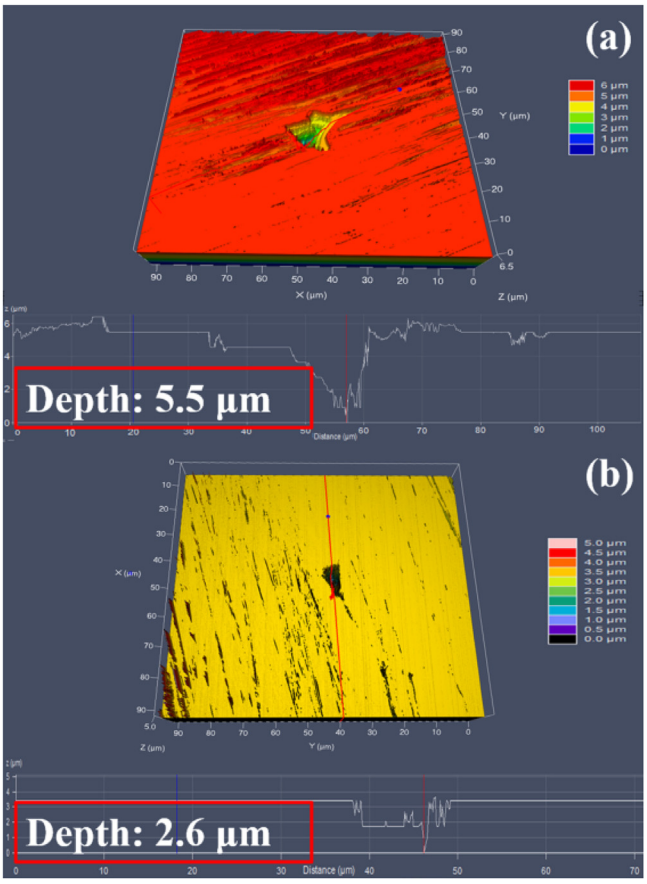

Fig. 4. Largest pit depth measured using CLSM on 2205 DSS (a) and 2205-Cu DSS (b) coupon surfaces after 14 days in *A. aceti* broth.

of immersion, 2205 DSS still had slightly more sessile cells than 2205-Cu DSS.

Fig. 4 shows the largest pits obtained using CLSM on 2205 DSS and 2205-Cu DSS coupon surfaces exposed to the *A. aceti* broth after 14 days of incubation. The largest pit depth on the 2205 DSS surface was 5.5 μm, larger than 2.6 μm for 2205-Cu DSS surface. In this work, the average largest pit depth was calculated by selecting the 10 largest pit depth values from 3 coupons for averaging. It was found that the averaged largest pit depth for 2205 DSS was 4.1 ± 1.2 μm vs. 1.9 ± 0.6 μm for 2205-Cu DSS. The pit depth data here clearly suggest that pitting corrosion was considerably mitigated on the surface of 2205-Cu DSS compared with 2205 DSS.

3.2. OCP

Fig. 5 shows the variation of E_{OCP} (OCP value) with the immersion time for 2205 DSS and 2205-Cu DSS coupons with and without *A. aceti*. The abiotic E_{OCP} of 2205 DSS was relatively stable throughout the 14-day test, while in the presence of *A. aceti*, the E_{OCP} shifted negatively, reaching −281 mV after 2 days of immersion. The E_{OCP} of 2205-Cu DSS showed a downward trend and reached −362 mV in the presence of *A. aceti* after 9 days. It then shifted in the positive direction reaching −276 mV after 14 days of immersion. The E_{OCP} of 2205-Cu DSS in the sterile medium was more positive compared to that of 2205-Cu DSS in the presence of *A. aceti*.

3.3. Potentiodynamic polarization

Fig. 6 gives the polarization curves of 2205 DSS and 2205-Cu DSS coupons in the sterile medium and in the presence of *A. aceti* after

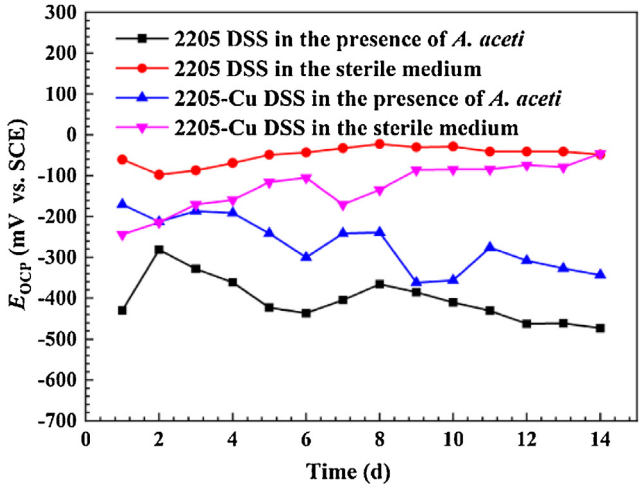

Fig. 5. Variations of E_{OCP} with incubation time for 2205 DSS and 2205-Cu DSS coupons in the sterile medium and in the *A. aceti* broth.

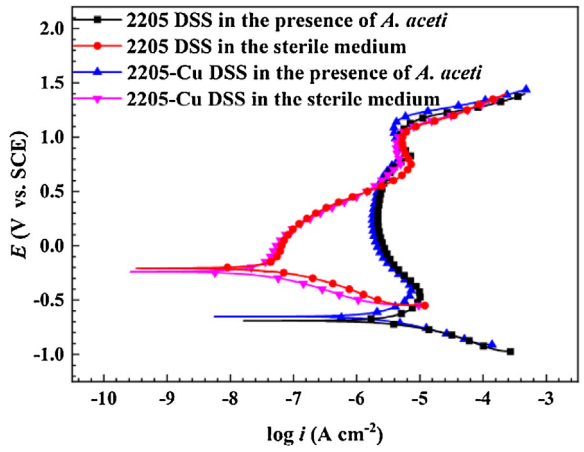

Fig. 6. The polarization curves at the end of the 14th day of incubation for 2205 DSS and 2205-Cu DSS in the sterile medium and in the *A. aceti* broth.

14 days of incubation. Table 2 shows the electrochemical corrosion parameters including corrosion potential (E_{corr}) and corrosion current density (i_{corr}) obtained from a Tafel analysis of the polarization curves. In the abiotic control, both i_{corr} values of 2205 DSS (0.14 ± 0.01 μA cm^{-2}) and 2205-Cu DSS (0.07 ± 0.03 μA cm^{-2}) were much lower than those in the biotic broth (3.69 ± 0.65 μA cm^{-2} for 2205 DSS, 0.42 ± 0.03 μA cm^{-2} for 2205-Cu DSS), indicating the occurrence of MIC caused by *A. aceti* [37,38]. Compared with that for 2205 DSS, the polarization curve of 2205-Cu DSS shifted to the left with the increase in E_{corr} value and the decrease of anodic reaction rate. In the *A. aceti* broth, the i_{corr} was 0.42 ± 0.03 μA cm^{-2} for 2205-Cu DSS, which was much lower than that for 2205 DSS (3.69 ± 0.65 μA cm^{-2}). The pitting corrosion potential E_{pit} of 2205-Cu DSS was higher than that of 2205 DSS in the presence of *A. aceti*. The results above demonstrated that 2205-Cu DSS inhibited MIC [39]. The corrosion inhibition efficiency (η_p) of 2205-Cu in the presence of *A. aceti* was 89% after the 14-day immersion based on the following equation [40]:

$$\eta_p = \frac{i_{corr(uninh)} - i_{corr(inh)}}{i_{corr(uninh)}} \times 100\% \quad (1)$$

where $i_{corr(uninh)}$ and $i_{corr(inh)}$ are the uninhibited (2205 DSS) and inhibited (2205-Cu DSS) corrosion current densities in the presence of *A. aceti*.

Table 2
The electrochemical corrosion parameters determined from the polarization curves of 2205 DSS and 2205-Cu DSS coupons after 14 days of incubation.

Sample	E_{corr}(mV vs. SCE)	i_{corr}(μA cm^{-2})	E_{pit}(mV vs. SCE)
2205 DSS in the sterile medium	−170 ± 51	0.14 ± 0.01	1323 ± 11
2205 DSS in the presence of *A. aceti*	−682 ± 18	3.69 ± 0.65	1268 ± 9
2205-Cu DSS in the sterile medium	−216 ± 31	0.07 ± 0.03	1322 ± 11
2205-Cu DSS in the presence of *A. aceti*	−658 ± 10	0.42 ± 0.03	1294 ± 57

Table 3
EIS parameters of 2205 DSS and 2205-Cu DSS in sterile medium and *A. aceti* broth.

Duration (d)	R_s(Ω cm^2)	C_b(μF cm^{-2})	R_f(kΩ cm^2)	C_{dl}(μF cm^{-2})	R_{ct}(kΩ cm^2)	$\sum\chi$ (×10^{-3})
2205-Cu DSS in the presence of *A. aceti*						
1	313 ± 152	24.9 ± 0.8	11.7 ± 2.1	13.3 ± 2.1	829 ± 312	5.33
5	203 ± 45	22.4 ± 2.4	7.5 ± 1.6	13.7 ± 2.0	825 ± 459	7.07
10	180 ± 20	24.3 ± 2.3	7.0 ± 1.0	15.3 ± 0.7	889 ± 271	7.61
14	140 ± 21	22.7 ± 0.6	6.1 ± 2.2	15.0 ± 0.1	1017 ± 88	1.07
2205 DSS in the presence of *A. aceti*						
1	144 ± 31	32.8 ± 7.0	4.8 ± 0.3	20.7 ± 4.1	827 ± 279	7.26
5	111 ± 3	26.8 ± 0.8	3.6 ± 0.1	19.4 ± 0.3	691 ± 70	1.20
10	115 ± 4	24.5 ± 0.9	3.9 ± 0.2	18.5 ± 0.1	460 ± 226	1.12
14	99 ± 10	23.9 ± 0.6	3.1 ± 0.3	20.1 ± 0.4	246 ± 204	1.39
2205-Cu DSS in the sterile medium						
1	383 ± 108	–	–	52.4 ± 20.4	405 ± 375	1.87
5	297 ± 79	–	–	17.1 ± 8.8	960 ± 184	3.26
10	216 ± 89	–	–	18.2 ± 9.8	899 ± 326	3.33
14	232 ± 76	–	–	19.8 ± 8.1	1103 ± 434	3.59
2205 DSS in the sterile medium						
1	243 ± 28	–	–	33.8 ± 2.7	545 ± 21	3.08
5	180 ± 14	–	–	27.8 ± 1.4	1021 ± 126	3.07
10	184 ± 22	–	–	26.0 ± 1.4	1187 ± 47	2.99
14	163 ± 4	–	–	26.1 ± 0.2	1180 ± 28	3.08

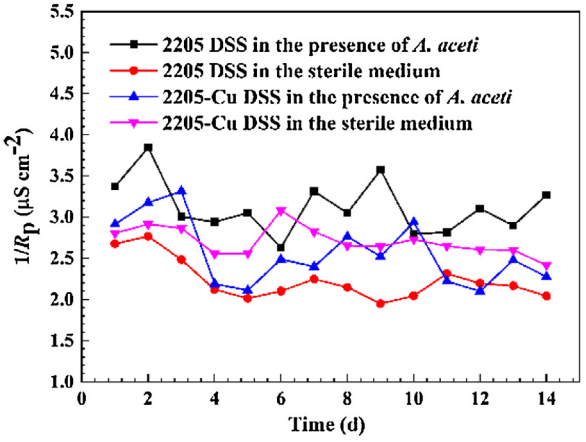

Fig. 7. Variations of $1/R_p$ with exposure time for 2205 DSS and 2205-Cu DSS coupons in the sterile medium and in the *A. aceti* broth.

3.4. LPR

In this work, $1/R_p$ was employed to describe the corrosion rates of 2205 DSS and 2205-Cu DSS coupons qualitatively. Fig. 7 shows the variation of $1/R_p$ with incubation time for both metals. In the presence of *A. aceti*, $1/R_p$ of 2205 DSS was higher than that in the sterile medium, indicating MIC by the APB. In the biotic medium, $1/R_p$ of 2205-Cu DSS was lower than that of 2205 DSS, indicating better corrosion resistance for 2205-Cu DSS. $1/R_p$ of 2205-Cu DSS decreased from 3.3 μS cm^{-2} on the 3rd day to 2.1 μS cm^{-2} on the 5th day, and then increased to 2.9 μS cm^{-2} after 10 days.

3.5. EIS

Fig. 8 exhibits the Bode and Nyquist plots of 2205 DSS and 2205-Cu DSS in the sterile medium and in the presence of *A. aceti*. The Nyquist plots diameters of 2205 DSS in the presence of *A. aceti* were smaller than that of 2205-Cu DSS, indicating better corrosion resistance for 2205-Cu DSS [41]. The physical models and the corresponding equivalent circuits are given in Fig. 9, where R_s represents the resistance of the solution, R_f the resistance of the film including biofilm and corrosion products, R_{ct} the charge transfer resistance. C_f and C_{dl} the capacitances for the film and electrical double layer, respectively. The correlated parameters from an EIS analysis of both metals in the presence of *A. aceti* are listed in Table 3. Variations of R_{ct} calculated from EIS data fitting are shown in Fig. 10. In the presence of *A. aceti*, R_{ct} of 2205-Cu DSS was 829 ± 312 kΩ cm^2. After 5 days, it decreased to 825 ± 459 kΩ cm^2, then gradually increased to 1017 ± 88 kΩ cm^2. In the presence of *A. aceti*, R_{ct} of 2205-Cu DSS was much higher than that of 2205 DSS. In the sterile medium, compared with the initial day, R_{ct} of 2205-Cu DSS increased to 960 ± 184 kΩ cm^2 after 5 days, then slightly dropped to 899 ± 326 kΩ cm^2. After 14 days, it was 1103 ± 434 kΩ cm^2. Obviously, in the abiotic broth, R_{ct} of 2205-Cu DSS was lower than that of 2205 DSS. η_R, which is the resistance-based corrosion inhibition efficiency, can be acquired by using the following equation [41]:

$$\eta_R = \frac{R_{ct(inh)} - R_{ct(uninh)}}{R_{ct(inh)}} \times 100\% \quad (2)$$

where $R_{ct(inh)}$ and $R_{ct(uninh)}$ represent the inhibited (2205-Cu DSS) and uninhibited (2205 DSS) charge transfer resistances, respectively. Table 4 shows that η_R reached 76% after 14 days of incubation.

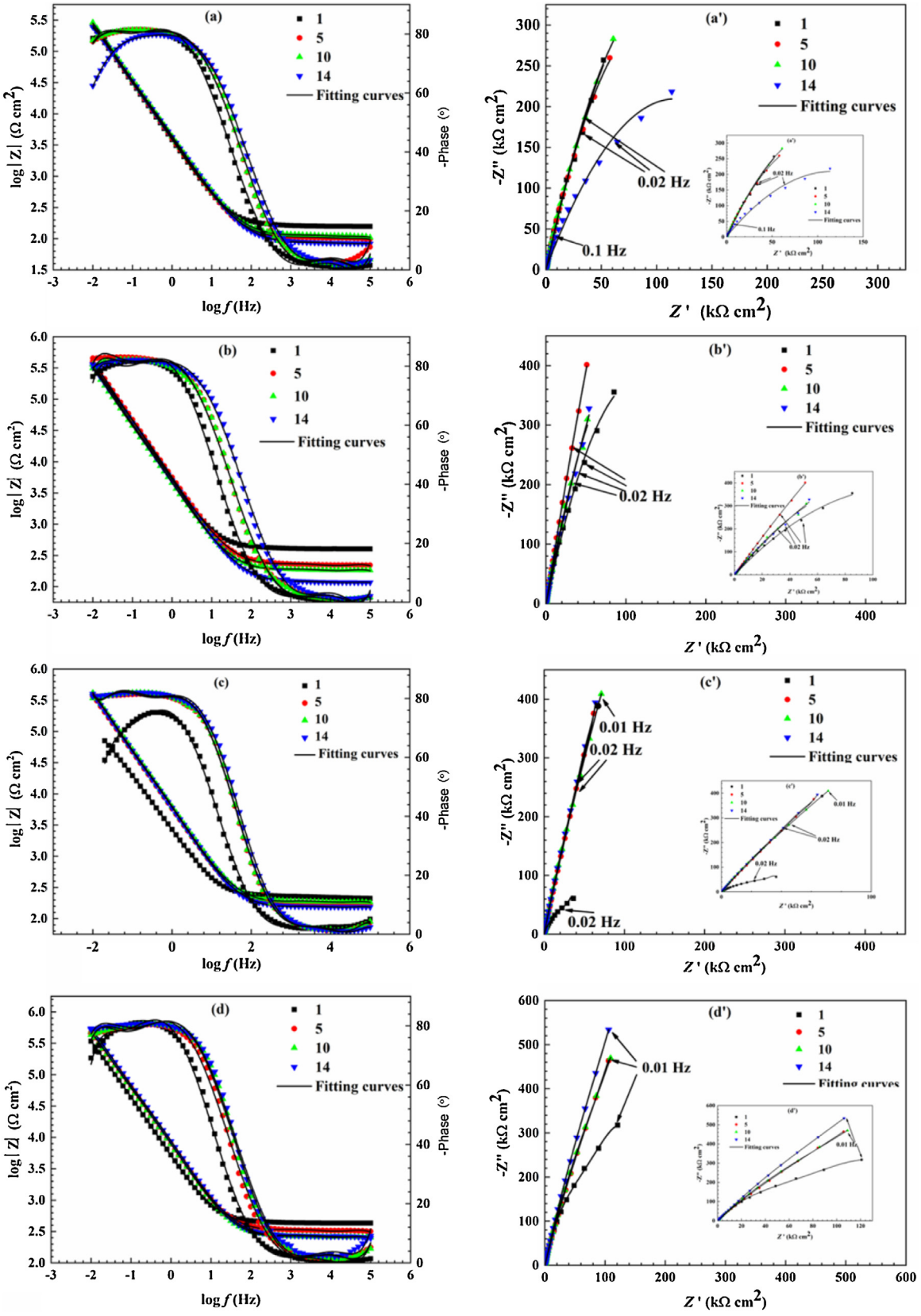

Fig. 8. Bode and Nyquist plots of 2205 DSS and 2205-Cu DSS: (a, a') 2205 DSS in the *A. aceti* broth (b, b') 2205-Cu DSS in the *A. aceti* broth (c, c') 2205 DSS in the sterile medium, (d, d') 2205-Cu DSS in the sterile medium.

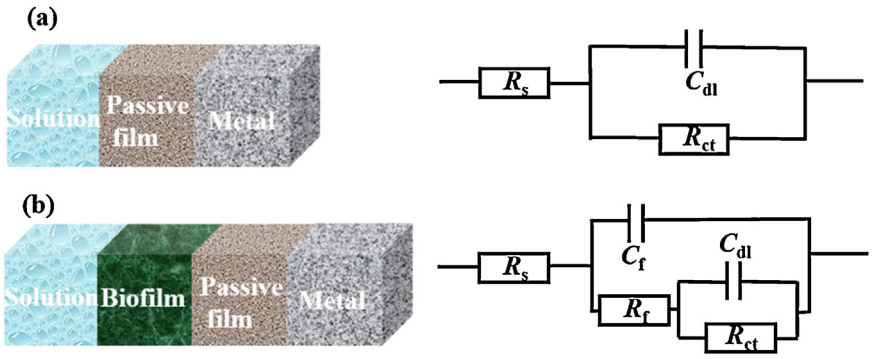

Fig. 9. Physical models and the corresponding equivalent circuits used for fitting the EIS data of 2205 DSS and 2205-Cu DSS coupons: (a) in the sterile medium and (b) in the *A. aceti* broth.

Table 4
Inhibition efficiency of 2205-Cu DSS against *A. aceti.*

Day	1	5	10	14
η_R (%)	0.3	16	48	76

Table 5
Relative atomic concentrations of the main elements on the surfaces of 2205 DSS and 2205-Cu DSS in the *A. aceti* broth after 14 days of incubation.

Sample	Atomic concentration (%)						
	C	N	O	Cl	Fe	Cr	Cu
2205 DSS	35.4	4.1	15.8	23.8	13.2	7.8	–
2205-Cu DSS	77.6	7.4	6.7	8.2	0	0	0.1

3.6. Analysis of corrosion products

The compositions of corrosion products on the surfaces of 2205 DSS and 2205-Cu DSS were analyzed by XPS. The corrosion product layer was detected after the coupons were incubated in the *A. aceti* inoculated medium for 14 days. Fig. 11 shows the survey spectra of XPS analysis for 2205 DSS and 2205-Cu DSS surfaces, both covered with biofilms. The relative atomic concentrations of the main elements are listed in Table 5. The main elements in the biofilms were C, N and O, and the total amounts of these 3 elements on both coupons exceeded 50%. Fe and Cr were not detected on the 2205-Cu DSS surface, while Cu was found. The high-resolution spectra of Cu 2*p* for 2205-Cu coupons after 14-day incubation in the *A. aceti* broth was shown in Fig. 12. Two peak components were found: CuO (933.2 eV) and $Cu(OH)_2$ (934.4 eV), which were the major corrosion products.

4. Discussion

The corrosion of the precipitated copper-rich phases formed during the aging treatment led to the release of the copper ions, providing the antimicrobial ability of 2205-Cu DSS. In Fig. 13, the concentration of Cu^{2+} released from 2205-Cu DSS increased gradually over time. The results of XPS analysis showed that Cu oxide were found in the corrosion product layer, which can be explained by the following reactions [42,43]:

$$Cu \rightarrow Cu^{2+} + 2e^- \quad (3)$$

$$Cu^{2+} + H_2O \rightarrow CuO + 2H^+ \quad (4)$$

$$8Cu + 2H_2O + O_2 \rightarrow 4Cu_2O + 4H^+ + 4e^- \quad (5)$$

$$2Cu_2O + 4H_2O + O_2 \rightarrow 4Cu(OH)_2 \quad (6)$$

Copper ions possess strong antibacterial and anti-biofilm properties [[44–46]]. Cu^{2+} ions can inhibit cell division, degrade DNA and

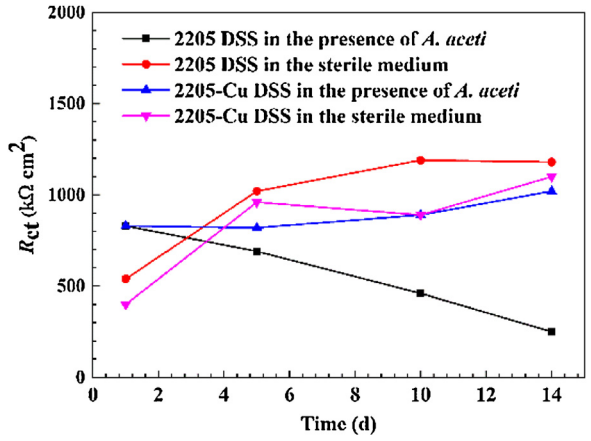

Fig. 10. Variations of R_{ct} measured from the EIS data for 2205 DSS and 2205-Cu DSS with and without *A. aceti.*

oxidize proteins, resulting in cell death [[47–50]]. In addition, Cu^{2+} ions can adhere to cell surface, changing the function and structure of enzymes. Cu^{2+} can destroy bacterial cell walls as well, leading to cytoplasm degradation and cell death [51]. The inoculated medium showed weak acidity due to the acetic acid produced by *A. aceti*. In the inoculated medium with 2205 DSS, the pH decreased to 5.64 ± 0.02 after 7 days from the initial pH of 6.76 ± 0.02 (Fig. 14). In contrast, due to the biofilm inhibition by the released Cu^{2+}, the acid production by the weakened biofilm decreased. Thus, the broth pH decreased to approximately 6.02 ± 0.01 (greater than 5.64 ± 0.02) after 7 days in the presence of 2205-Cu DSS, demonstrating its inhibition of the *A. aceti* biofilm.

It is well accepted that biofilms are responsible for MIC [13,14]. Therefore, inhibiting biofilms is an effective way to suppress MIC. The largest pit depth detected on the 2205-Cu DSS surface was 2.6 μm, which was much smaller than that of 2205 DSS (5.5 μm), indicating that Cu^{2+} released from 2205-Cu DSS inhibited the *A. aceti* biofilm's production of acetic acid, thus inhibited the MIC of 2205-Cu DSS by the APB.

The inhibition of MIC by Cu^{2+} released by 2205-Cu DSS during its corrosion was also demonstrated by the results of electrochemical tests. Cu^{2+} impacted the growth and attachment of the *A. aceti* biofilm, thereby affecting the state of the metal surface. OCP directly correlated with the surface reaction occurred on the 2205-Cu DSS surface [52]. As shown in Fig. 5, the E_{OCP} value of 2205-Cu DSS in the abiotic medium decreased to −362 mV on the 9th day, and then shifted in the positive direction. It was more unstable than that of the 2205 DSS. A more negative OCP means that the working electrode has a higher thermodynamic tendency to lose electrons. Fig. 5 shows this trend, in which biotic E_{OCP} curves are more nega-

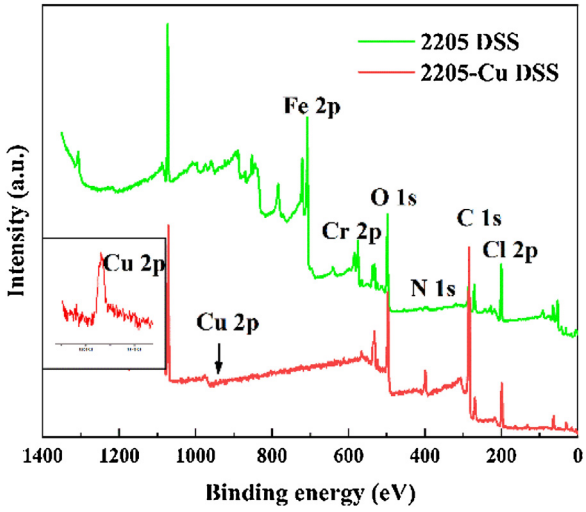

Fig. 11. Survey spectra of XPS analysis for 2205 DSS and 2205-Cu DSS after 14-day incubation in *A. aceti* broth.

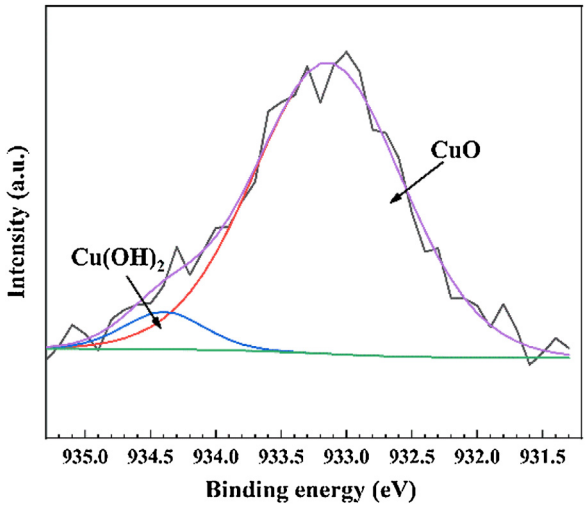

Fig. 12. XPS spectra of Cu 2p for 2205-Cu DSS coupons after 14-day incubation in *A. aceti* broth.

tive than abiotic E_{OCP}. It should be noted that the actual corrosion rate depends on corrosion kinetics. In Table 3, R_{ct} of 2205-Cu DSS in the biotic medium was much higher than that of 2205 DSS, indicating that the transfer of charge from the metal surface to the biofilm was greatly hampered. On the first day, η_R was 0.3%, then gradually increased, and reached 76% after 14 days. This is not very far from the 89% efficiency based on i_{corr}. This result implied that MIC caused by *A. aceti* was considerably inhibited by the addition of Cu in 2205 DSS. Fig. 15 shows the schematic illustration of the MIC resistant mechanism of 2205-Cu DSS against MIC caused by *A. aceti*. In the presence of the acetic acid secreted by *A. aceti*, the passive film on stainless steel can be destroyed, causing its corrosion [53,54]. Cheng et al. investigated the properties of the passive films on 316 L SS and 2205 DSS, confirming that acetic acid can attack the passive films [55,56]. Underneath an *A. aceti* biofilm, the passive film suffers from the attack by a higher local concentration of acetic acid than that in the bulk fluid phase because the sessile cell volumetric density is often 10^2 or higher than that in the bulk-fluid phase [57]. Once the passive film is compromised, the Cu-rich phase as well as the rest of the metal is attacked, releasing antibacterial Cu ions. With the release of Cu^{2+}, the sessile cells on the surface of 2205-Cu DSS are considerably inhibited, thus mitigating the MIC due to less production of acetic acid by the inhibited APB biofilm. This delayed killing of sessile cells is reflected by the increased dead cell amount after 14 days of incubation vs. 7 days of incubation in Fig. 2.

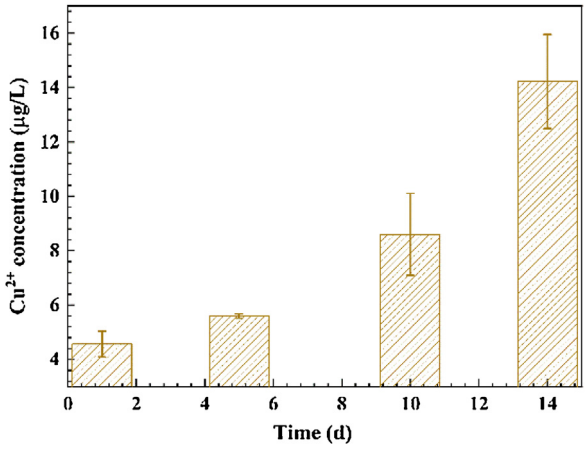

Fig. 13. The release of Cu^{2+} from 2205-Cu DSS in the *A. aceti* broth vs. exposure time.

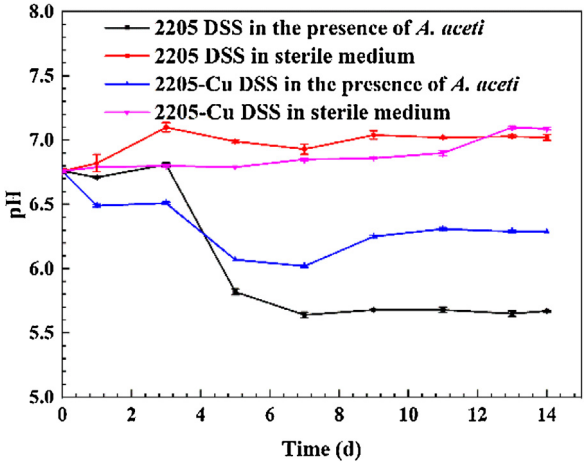

Fig. 14. Variations of pH for 2205 DSS and 2205-Cu DSS in sterile medium and *A. aceti* broth.

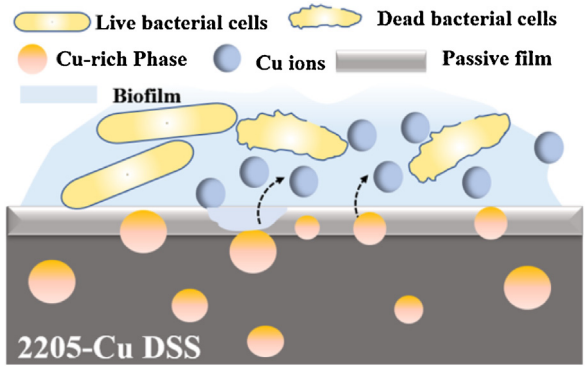

Fig. 15. Schematic illustration of MIC resistance mechanism for 2205-Cu DSS.

5. Conclusion

The anti-biofilm ability and corrosion resistance of 2205-Cu DSS vs. 2205 DSS (control) were investigated using acid producing bacterium *A. aceti*. The results from electrochemical tests indicated that 2205-Cu DSS considerably inhibited the pitting corrosion caused by the *A. aceti*. Due to the releasing of Cu^{2+} from the 2205-Cu DSS

matrix, it exhibited a good antibiofilm ability as evidenced by the CLSM images of live and dead cells on the metal surfaces. The live sessile cells on 2205-Cu DSS were 4-fold less than those on 2205 DSS, while the dead sessile cells on the 2205-Cu DSS surface were 2 orders of magnitude more than those on the 2205 DDS surface after 14 days of incubation, resulting in the inhibition of the *A. aceti* biofilm and its MIC. The pits observed on the surface of 2205-Cu DSS were smaller and shallower compared to those on the 2205 DSS surface, demonstrating that the 2205-Cu DSS possessed MIC pitting corrosion resistance.

Acknowledgements

This work was supported by the National Natural Science Foundation of China (No. U1608254), Shenzhen Science and Technology Research Funding (No. JCYJ20160608153641020), the Open Fund of State Key Laboratory of Comprehensive Utilization of Low-Grade Refractory Gold Ores (Nos. ZJKY2017 (B) KFJJ01 and ZJKY2017 (B) KFJ02).

References

[1] R. Lai, Y. Cai, Y. Wu, F. Li, X. Hua, Mater. Process. Technol. 231 (2016) 397–405.
[2] V. Muthupandi, P.B. Srinivasan, S.K. Seshadri, S. Sundaresan, Mater. Sci. Eng. A 358 (2003) 9–16.
[3] S.M. Yang, Y.C. Chen, Y.T. Pan, D.Y. Lin, Mater. Sci. Eng. C 63 (2016) 376–383.
[4] H.Y. Ha, M.H. Jang, T.H. Lee, J. Moon, Corros. Sci. 89 (2014) 154–162.
[5] J. Olsson, M. Snis, Desalination 205 (2007) 104–113.
[6] C. Örnek, D.L. Engelberg, Mater. Sci. Eng. A 666 (2016) 269–279.
[7] E. Zhou, H. Li, C. Yang, J. Wang, D. Xu, D. Zhang, T. Gu, Int. Biodeterior. Biodegrad. 127 (2018) 1–9.
[8] Y. Zhao, E. Zhou, Y. Liu, S. Liao, Z. Li, D. Xu, T. Zhang, T. Gu, Corros. Sci. 126 (2017) 142–151.
[9] P. Li, Y. Zhao, Y. Liu, Y. Zhao, D. Xu, C. Yang, T. Zhang, T. Gu, K. Yang, J. Mater. Sci. Technol. 33 (2017) 723–727.
[10] Y. Zhao, E. Zhou, D. Xu, Y. Yang, Y. Zhao, T. Zhang, T. Gu, K. Yang, F. Wang, Corros. Sci. 143 (2018) 281–291.
[11] X. Li, D. Zhang, Z. Liu, Z. Li, C. Du, C. Dong, Nat. News 527 (2015) 441–442.
[12] F.M. AlAbbas, S.M. Bhola, J.R. Spear, D.L. Olson, B. Mishra, Eng. Fail. Anal. 33 (2013) 222–235.
[13] R. Jia, D. Yang, J. Xu, D. Xu, T. Gu, Corros. Sci. 127 (2017) 1–9.
[14] D. Xu, E. Zhou, Y. Zhao, H. Li, Z. Liu, D. Zhang, C. Yang, H. Lin, X. Li, K. Yang, J. Mater. Sci. Technol. 34 (2018) 1325–1336.
[15] D. Xu, R. Jia, Y. Li, T. Gu, World J. Microbiol. Biotechnol. 33 (2017) 97.
[16] H. Li, C. Yang, E. Zhou, C. Yang, H. Feng, Z. Jiang, D. Xu, T. Gu, K. Yang, J. Mater. Sci. Technol. 33 (2017) 1596–1603.
[17] L. Nan, D. Xu, T. Gu, X. Song, K. Yang, Mater. Sci. Eng. C. 48 (2015) 228–234.
[18] D. Xu, Y. Li, F. Song, T. Gu, Corros. Sci. 77 (2013) 385–390.
[19] R. Jia, D. Yang, H.B. Abd Rahman, T. Gu, Corros. Sci. 139 (2018) 301–308.
[20] R. Jia, J.L. Tan, P. Jin, D.J. Blackwood, D. Xu, T. Gu, Corros. Sci. 130 (2018) 1–11.
[21] R. Jia, D. Yang, D. Xu, T. Gu, Front. Microbiol. 8 (2017) 1–9.
[22] Y. Li, D. Xu, C. Chen, X. Li, R. Jia, D. Zhang, W. Sand, F. Wang, T. Gu, J. Mater. Sci. Technol. 34 (2018) 1713–1718.
[23] Y. Dong, B. Jiang, D. Xu, C. Jiang, Q. Li, T. Gu, Bioelectrochemistry 123 (2018) 34–44.
[24] B.J. Little, R.I. Ray, R.K. Pope, Encyclopedia of Materials: Science and Technology, Oxford, 2001, pp. 533–537.
[25] B.J. Little, T.L. Gerke, R.I. Ray, J.S. Lee, Mineral Scales and Deposits, Elsevier, Amsterdam, 2015, pp. 107–122.
[26] J.W. Sowards, C.H.D. Williamson, T.S. Weeks, J.D. McColskey, J.R. Spear, Corros. Sci. 79 (2014) 128–138.
[27] J.W. Sowards, E. Mansfield, Corros. Sci. 87 (2014) 460–471.
[28] C. Andrés-Barrao, M.M. Saad, M.-L. Chappuis, M. Boffa, X. Perret, R. Ortega Pérez, F. Barja, J. Proteomics 75 (2012) 1701–1717.
[29] K. Sakurai, H. Arai, M. Ishii, Y. Igarashi, J. Biosci. Bioeng. 113 (2012) 343–348.
[30] K. Sakurai, S. Yamazaki, M. Ishii, Y. Igarashi, H. Arai, J. Biosci. Bioeng. 115 (2013) 32–36.
[31] Y. Kryachko, S.M. Hemmingsen, Curr. Microbiol. 74 (2017) 870–876.
[32] T. Gu, J. Microb. Biochem. Technol. 06 (2014).
[33] D. Sun, M. Babar Shahzad, M. Li, G. Wang, D. Xu, Mater. Technol. 30 (2014) 90–95.
[34] J. Liu, R. Jia, E. Zhou, Y. Zhao, W. Dou, D. Xu, K. Yang, T. Gu, Int. Biodeterior. Biodegrad. 132 (2018) 132–138.
[35] J. Xia, C. Yang, D. Xu, D. Sun, L. Nan, Z. Sun, Q. Li, T. Gu, K. Yang, Biofouling 31 (2015) 481–492.
[36] Y. Lou, L. Lin, D. Xu, S. Zhao, C. Yang, J. Liu, Y. Zhao, T. Gu, K. Yang, Int. Biodeterior. Biodegrad. 110 (2016) 199–205.
[37] R. Jia, D. Wang, P. Jin, T. Unsal, D. Yang, J. Yang, D. Xu, T. Gu, Corros. Sci. 153 (2019) 127–137.
[38] T. Unsal, R. Jia, S. Kumseranee, S. Punpruk, T. Gu, Eng. Fail. Anal. 100 (2019) 544–555.
[39] X. Shi, W. Yan, D. Xu, M. Yan, C. Yang, Y. Shan, K. Yang, J. Mater. Sci. Technol. 34 (2018) 2480–2491.
[40] N.O. San, H. Nazır, G. Dönmez, Corros. Sci. 79 (2014) 177–183.
[41] J. Zhao, Z. Zhai, D. Sun, C. Yang, X. Zhang, N. Huang, X. Jiang, K. Yang, Mater. Sci. Eng. C 100 (2019) 396–410.
[42] S. Zhang, C. Yang, G. Ren, L. Ren, Mater. Process. Rep. 30 (2015) B126–B132.
[43] H. Liu, D. Xu, K. Yang, H. Liu, Y.F. Cheng, Corros. Sci. 132 (2018) 46–55.
[44] M. Vincent, P. Hartemann, M. Engels-Deutsch, Int. J. Hyg. Environ. Health 219 (2016) 585–591.
[45] M.G. Schmidt, R.E. Tuuri, A. Dharsee, H.H. Attaway, S.E. Fairey, K.T. Borg, C.D. Salgado, B.E. Hirsch, Am. J. Infect. Control 45 (2017) 642–647.
[46] N. Thokala, C. Kealey, J. Kennedy, D.B. Brady, J.B. Farrell, Mater. Sci. Eng. C 78 (2017) 1179–1186.
[47] H. Strahl, L.W. Hamoen, Proc. Natl. Acad. Sci. 107 (2010) 12281–12286.
[48] Y.M. Zhang, C.O. Rock, Nat. Rev. Microbiol. 6 (2008) 222–233.
[49] S.S. Justice, D.A. Hunstad, L. Cegelski, S.J. Hultgren, Nat. Rev. Microbiol. 6 (2008) 162–168.
[50] H.N. Abdelhamid, H.F. Wu, TrAC Trends Anal. Chem. 65 (2015) 30–46.
[51] A.K. Chatterjee, R. Chakraborty, T. Basu, Nanotechnology 25 (2014) 1–12.
[52] I.T. Hong, C.H. Koo, Mater. Sci. Eng. A 393 (2005) 213–222.
[53] X. Gao, J. Tang, Y. Zuo, Y. Tang, J. Xiong, Corros. Sci. 51 (2009) 1822–1827.
[54] S. Li, Y. Zuo, Y. Tang, X. Zhao, Appl. Surf. Sci. 321 (2014) 179–187.
[55] X. Cheng, X. Li, C. Du, Chin. Sci. Bull. 54 (2009) 2239–2246.
[56] X. Cheng, X. Li, C. Dong, Int. J. Miner. Metall. Mater. 16 (2009) 170–176.
[57] H. Li, D. Xu, Y. Li, H. Feng, Z. Liu, X. Li, T. Gu, K. Yang,PLoS One 10 (2015), e0136183.